# Exploring Biorelevant Conditions and Release Profiles of Ritonavir from HPMCAS-Based Amorphous Solid Dispersions

***Pradnya Bapat,[1] Robert Schwabe,[2] Shubhajit Paul,[2], Yin-Chao Tseng,[2] Cameron Bergman,[1] Lynne S. Taylor.[1]****

1. Department of Industrial and Molecular Pharmaceutics, College of Pharmacy, Purdue University, West Lafayette, Indiana 47907, United States

2. Material and Analytical Sciences, Research and Development, Boehringer Ingelheim Pharmaceuticals, Inc., Ridgefield, Connecticut 06877, United States

*Correspondence: Lynne S. Taylor

Telephone: +1-765-496-6614; Fax: +1-765-494-6545)

Email address: lstaylor@purdue.edu

## 1. Abstract

Development of a release test for amorphous solid dispersions (ASDs) that is in vivo predictive is essential to identify optimally performing formulations early in development. For ASDs containing an enteric polymer, consideration of buffer properties is essential. Herein, release rates of hydroxypropyl methyl cellulose acetate succinate (HPMCAS) and ritonavir from ASDs with a 20% drug loading were compared in phosphate and bicarbonate buffers with different molarities, at pH 6.5. The bioaccessibility of ritonavir from the ASD in the tiny-TIM apparatus was also evaluated and compared to that of the crystalline drug. The surface pH at the dissolving solid: solution interface was evaluated using a pH-sensitive fluorescence probe for HPMCAS and ASD compacts in phosphate and bicarbonate buffers. Drug and polymer were found to release congruently in all buffer systems, indicating that the polymer controlled the drug release. Release was slowest in 10 mM bicarbonate buffer, and much faster in phosphate buffers with molarities typically used in release testing (20-50 mM). Release from the 10 mM bicarbonate buffer was matched in a 5 mM phosphate buffer. The surface pH of HPMCAS and HPMCAS:ritonavir ASDs was found to be lower than the bulk solution pH, where surface pH differences largely explained release rate differences seen in the different buffer systems. Ritonavir was highly bioaccessible from the ASD, as assessed by the tiny-TIM system, and much less bioaccessible when crystalline drug was used. The observations highlight the need for continued development of biorelevant assays tailored for ASD formulation assessment.

Keywords: amorphous solid dispersion; surface pH; biorelevancy; release performance

TOC Graphic

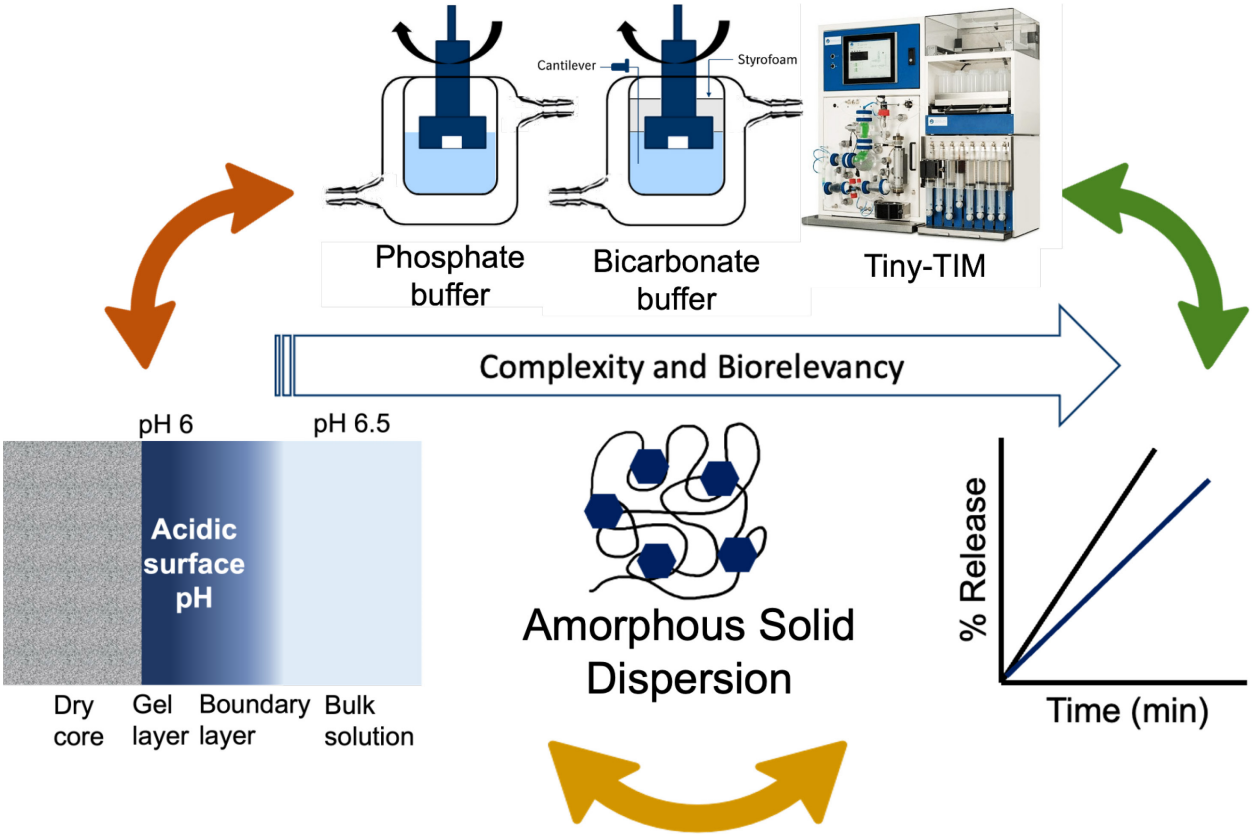
Cantilever
Styrofoam
Phosphate buffer
Bicarbonate buffer
Tiny-TIM
Complexity and Biorelevancy
pH 6
pH 6.5
Acidic surface pH
Dry core
Gel layer
Boundary layer
Bulk solution
Amorphous Solid Dispersion
% Release
Time (min)

## 2. Introduction

Amorphous solid dispersions (ASDs) are widely used to improve the bioavailability of poorly soluble drugs.[1–14] An amorphous solid dispersion is a molecular mixture of a drug and a polymer, yielding a single phase homogeneous blend. The amorphous form of a drug has a transiently higher solubility than the equilibrium crystalline solubility, and consequently, supersaturated solutions can be generated following dissolution under non-sink conditions. However, if crystallization occurs, the extent of supersaturation is decreased.[2,9,15,16] ASD polymers ideally inhibit crystallization in the solid and solution phases, and consequently improve drug release relative to neat amorphous drug.

Hydroxypropyl methylcellulose acetate succinate (HPMCAS), is a commonly used enteric ASD polymer.[14,17,18] Congruent release of drug and polymer has been noted from ASDs with HPMCAS, in particular at lower drug loadings, suggesting that drug release is controlled by the polymer dissolution rate.[3,19,20] Given the key role played by the polymer in controlling drug release from an ASD, determination of factors that impact the polymer dissolution rate is key to understand the overall release profiles of ASD formulations. Ionization of carboxylic acid groups is the critical step in enteric polymer dissolution, since it leads to hydration, solubilization and the subsequent dissolution of the polymer chains.[3,21,22] Enteric polymers tend to have an acidic micro-environment at the dissolving interface due to liberation of protons following ionization of carboxylic acid groups.[23–28] Hence, dissolution media factors such ionic strength, buffer capacity and buffer species $pK_a$, as well as pH impact polymer dissolution rate.[3,21,23–29] Drug loading and drug physico-chemical properties also impact polymer release.[3]

Biorelevant media, such as fasted state simulated gastric fluid (FaSSGF), fasted state simulated intestinal fluid (FaSSIF), and fed state simulated intestinal fluid (FeSSIF) are frequently

employed in release studies to better understand the effect of bile salts and other digestive components.[30] However, biorelevant media may not adequately simulate *in vivo* conditions as far as buffer capacity is concerned. *In vivo* intestinal fluid buffer capacity values are very low, being in the range of 2-8 mM/ΔpH in the fasted state and 3-15 mM/ΔpH in the fed state gastrointestinal (GI) tract.[3,31–33] The buffer capacity of FaSSIF was reported to be around 10 mM/ΔpH and that of FeSSIF was around 25 mM/ΔpH.[30,31] Several studies have compared the effect of phosphate versus bicarbonate buffers on the dissolution rate of BCS II weak acids.[34,35] For indomethacin, much higher dissolution rates were observed in FaSSIF compared to a more physiologically-relevant bicarbonate buffer, for a fixed pH.[36] This was attributed to differences in media buffer capacity.

Bicarbonate is the pH modifying agent in the small intestine.[34–39] Thus, bicarbonate buffer is the most biorelevant testing media for mimicking the upper small intestine in terms of factors such as buffer capacity and species. The pH of a bicarbonate buffer depends on the concentration of carbonate ions, carbonic acid, dissolved $CO_2$, and the partial pressure of $CO_2$ in the headspace.[40] Studies show that it is possible to generate a stable bicarbonate buffer by continuous sparging of $CO_2$ to maintain the buffer species concentration as well as the pH. However, it is not particularly convenient to use bicarbonate buffer for *in vitro* release testing. To broaden the use of bicarbonate buffers, Sugano and coworkers developed a floating lid apparatus where a foamed styrol sheet was inserted above the surface of the bicarbonate buffer solution in a USP II apparatus. This decreased the headspace and delayed release of $CO_2$. The method was user-friendly and maintained the pH over the duration of the experiment, making the use of bicarbonate buffer more convenient in the lab.[39,41]

It has been noted that bicarbonate buffer has a higher buffer capacity in bulk solution as compared to in the diffusion boundary layer at the interface between the dissolving solid and solution. This is due to the slow kinetics of hydration and dehydration reactions of $CO_2$ and $H_2CO_3$ relative to the diffusion rate of species. Hence, the effective $pK_a$ of bicarbonate in the boundary layer lies between 4 to 5 even though its apparent $pK_a$ is 6.04.[40]

Since dissolution ultimately happens *in vivo*, it is also important to understand the intricacies of the GI tract beyond simply using bicarbonate buffer. Various GI factors such as pH, buffer capacity, bile salts, surface tension, motility, osmolality, total protein content, pepsin etc. should be taken into consideration for understanding intraluminal performance of dosage forms.[42] The pH values of the luminal fluids are highly dynamic, and have been reported to range from 5.0 to 8.4 in comparison to the static values of biorelevant media (pH 6.8 in SIF and pH 6.5 in FaSSIF).[35] Also, postprandially the small intestine creates various motor patterns termed as migrating motor complexes (MMC) to mix the contents with chyme and intestinal fluids, and expose them uniformly to the mucosal tissue for absorption. Phase III of MMC has a characteristic feature of increasing the pH in the antroduodenal region i.e. rapid alkalization and duodenal phase III activates the release of electrogenic chloride and bicarbonates in the antral lumen.[43] It was also demonstrated from human intestinal fluid (HIF) samples collected postprandially that the solubilizing capacity of HIF is highly time dependent and pH plays an important role in the dissolution of ionizable drugs in the fed state.[44,45] These observations demonstrate that it is important to take into account the dynamic pH, as well as the low buffer capacity of GI fluids and perform *in vitro* studies in a dynamic set-up for better *in vitro in vivo* correlation (*IVIVC).*[31] This has led to the development and utilization of more complex *in vitro* testing systems. The TIM intestinal model is a computer-controlled dynamic gastro-intestinal

model which simulates all the processes of upper GI tract. Tiny-TIM is a benchtop version of TIM which has a simulated pressure-controlled gastric compartment and an intestinal compartment. The use of the tiny-TIM as a predictive tool for bioavailability of a variety of formulations has been discussed in the literature.[46–52]

The goal of this study was to investigate the release of neat HPMCAS and HPMCAS-based ASDs in increasingly biorelevant conditions. First, we compared the impact of low and high buffer capacity media on the dissolution of an ASD of a weakly basic drug, ritonavir (RTV) at a 20% drug loading (DL) in pH 6.5 phosphate buffer. We performed surface normalized release experiments using Wood's apparatus. Next, the drug and the polymer release were measured in bicarbonate buffer media. The floating lid method developed by Sugano et al[39,41] was adapted to the Wood's apparatus dissolution test. This approach maintained a constant pH for the experimental duration by minimizing $CO_2$ release. Finally, the release of a RTV: HPMCAS 20% drug loading (DL) ASD was evaluated using the tiny-TIM and the % of bioaccessible drug was compared for the ASD and a crystalline reference sample at a 100 mg dose. To confirm the role of interfacial pH as a factor in the release rate of components from the ASD, a fluorescence method was developed to determine the pH gradient across the boundary layer of an HPMCAS/ASD compact immersed in different buffers.

## 3. Materials

Ritonavir (RTV) was purchased from ChemShuttle (Jiangsu, China). Hydroxypropyl methyl cellulose acetate succinate (HPMCAS AQOAT -MF) was supplied by Shin-Etsu (Tokyo, Japan). Fluorescein isothiocyanate (FITC) and rhodamine 6G (R6G) were purchased from Sigma-Aldrich Co. (MO, U.S.A.). Methanol (MeOH), dichloromethane (DCM), acetonitrile (ACN), tetrahydrofuran (THF), phenol, sulfuric acid, trifluoroacetic acid (TFA), formic acid (FA), sodium

hydroxide (NaOH), sodium chloride (NaCl), triethylamine (TEA), sodium phosphate dibasic anhydrous ($Na_2HPO_4$), and sodium phosphate monobasic monohydrate ($NaH_2PO_4.H_2O$) were purchased from Fisher Chemicals (Fair Lawn, NJ, USA). Hydrochloric acid (HCl) and sodium bicarbonate ($NaHCO_3$) were supplied by Merck (USA). α-Amylase from Bacillus sp., lipase from *Rhizopus oryzae*, pepsin, pancreatin, sodium acetate trihydrate, glacial acetic acid, calcium chloride dihydrate ($CaCl_2 \cdot 2H_2O$), bile extract porcine powder, hydroxypropyl methyl cellulose (HPMC), gastric electrolyte stock were purchased from Sigma-Aldrich Co. (MO, U.S.A.). Chemical structures of RTV, HPMCAS, FITC and R6G are shown in Figure 1. Various buffer solutions used in this study are summarized in Table 1. High performance liquid chromatography (HPLC) grade ultrapure water was used for preparation of all buffers and mobile phases.

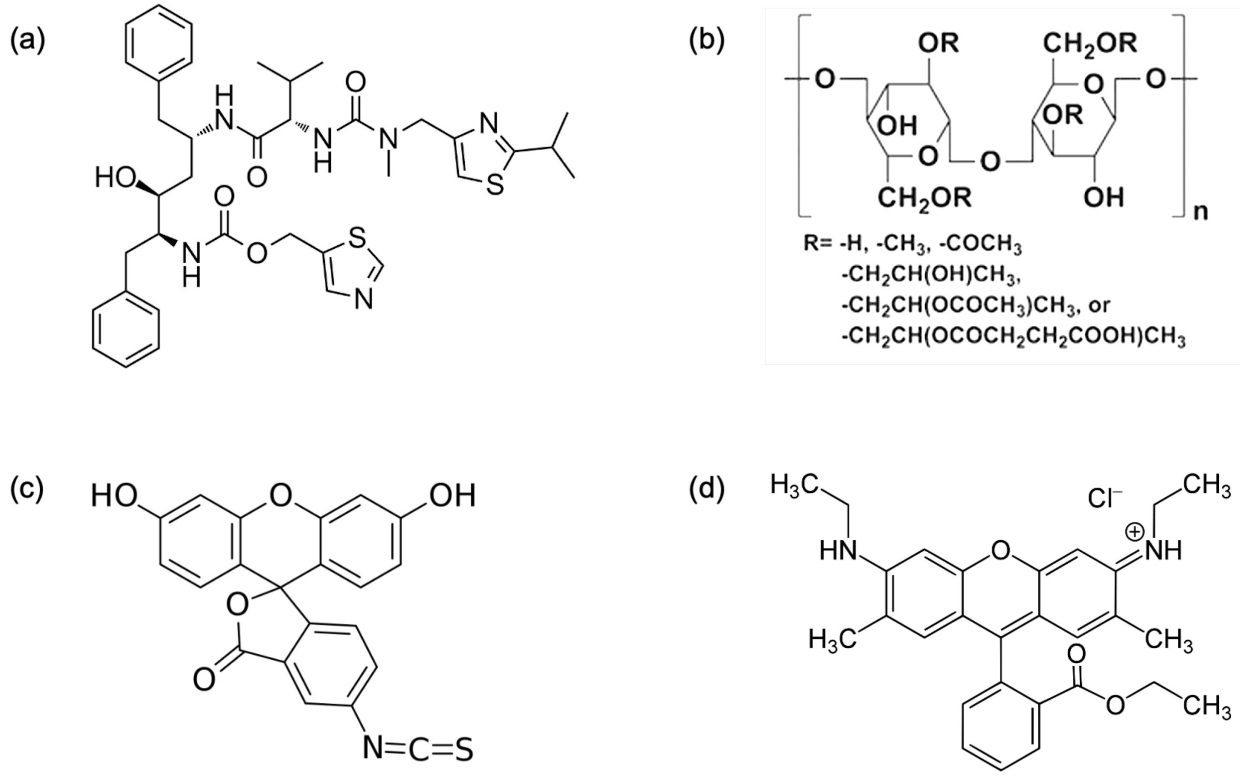


**Figure 1. Chemical structures of (a) ritonavir (RTV), (b) hydroxypropyl methyl cellulose acetate succinate (HPMCAS) (c) fluorescein isothiocyanate (FITC) (d) rhodamine 6G (R6G).**

**Table 1. Media used in the study with their buffer concentrations and capacities**

| Media | Buffer Concentration (mM) | Buffer capacity (mM/ΔpH) |
|---|---|---|
| pH 6.5 phosphate buffer | 5 | 1.9 |
| pH 6.5 phosphate buffer | 10 | 4.0 |
| pH 6.5 phosphate buffer | 20 | 8.7 |
| pH 6.5 phosphate buffer | 50 | 23.8 |
| pH 6.5 bicarbonate buffer | 10 | 4.4 |
| pH 6.5 bicarbonate buffer | 20 | 8.8 |

## 4. Methods

### 4.1. Analysis of Ritonavir Concentration

A high performance liquid chromatography (HPLC) method was developed to quantify the concentration of ritonavir. An Ascentis® Express (Sigma-Aldrich, St. Louis, MO) 90 Å C18 column with dimensions of 15 cm × 4.6 mm and particle size of 5 µm was used with a mobile phase of 50:50 v/v water: ACN with 0.1% TFA at 1 mL/min. The injection volume was 80 µL and the drug was detected at an ultraviolet (UV) wavelength of 210 nm. Standard curves were prepared in triplicate over the concentration range of 1-50 µg/mL with an $R^2$ of 0.999.

### 4.2. HPLC Analysis of HPMCAS

The concentration of HPMCAS was analyzed using HPLC and an evaporative light scattering detector (ELSD). A Shodex RS pak DS-413 column was used for the analysis. A gradient method was developed using a mobile phase of 0.1% FA in water and 0.1% FA in ACN at a flow rate of 0.5 mL/min with an injection volume of 80 µL. The method details for various systems are summarized in Table S1. A continuous flow of high-pressure liquid nitrogen at a rate of 1.5 standard L/min was required for the ELSD detector. The nebulizer temperature was set to 80 ºC and the evaporator temperature set to 85 ºC. Standard curves were prepared in triplicate over the concentration range of 1-250 µg/mL with an $R^2$ of 0.999.

4.3. Preparation of Amorphous Solid Dispersions

HPMCAS-based ASDs of ritonavir were prepared using a rotary evaporator (Hei-VAP Core rotary evaporator, Heidolph Instruments, Schwabach, Germany) equipped with an Ecodyst EcoChyll S cooler (Ecodyst, Apex, NC, USA). Briefly, ritonavir and HPMCAS were dissolved in 1:2 v/v MeOH: DCM and the solvent was evaporated on a rotary evaporator with a water bath maintained at 50 ºC. The ASDs were dried overnight under vacuum, cryomilled using a 6750 Freezer/Mill (SPEX SamplePrep, Metuchen, NJ) and sieved to obtain the particle size fraction in the range of 106-250 µm. The amorphous nature of ASDs was cofirmed using powder x-ray diffraction (PXRD) (Figure S1).

4.4. Surface Area Normalized Dissolution Rate Experiments

Intrinsic dissolution rate (IDR) type experiments were performed using Wood's apparatus (Agilent Technologies, Santa Clara, CA) for neat HPMCAS and RTV: HPMCAS ASDs in various media. 100 mg of the powder was added into the die (diameter of 8 mm and surface area of 0.5 $cm^2$) and compressed using a Carver press (Carver, Wabash, IN) under a pressure of 1500 psi held for one minute. The die was then attached to the rotating spindle and rotated at 100 rpm. The entire assembly was inserted into a jacketed beaker containing 100 mL of the dissolution medium maintained at 37 °C and connected to a water bath. Samples were taken at 5-minute intervals up to 30 minutes and at 10-minute intervals up to 60 minutes. Samples were replenished with fresh media. Drug and polymer were analyzed with HPLC as described in sections 3.1 and 3.2 respectively. The normalized release rate of the drug and polymer is calculated from equation 1.

$$R = \frac{k \times V}{S \times x} \qquad \text{(eq. 1)}$$

where $k$ is the slope of the regression line, $V$ is the volume of dissolution medium (100 mL), $S$ is the surface area of the compact exposed to the dissolution medium (0.5 $cm^2$) and $x$ is the weight fraction of each component.

4.5. Floating Lid Method Adapted to Wood's Apparatus

The floating lid set-up described by Sugano and coworkers[39,41] was adapted. Briefly, 100 mL of freshly prepared pH 6.5 bicarbonate buffer was added to the jacketed beaker which was attached to a water bath maintained at 37 ºC. A low-temperature polystyrene foam moisture-resistant insulation sheet was fitted inside the beaker immediately above the surface of the buffer to decrease the headspace and minimize $CO_2$ loss from the solution. The pH was monitored every minute for first 10 minutes and then every 5 minutes for up to 1 hour using a calibrated pH probe (Mettler Toledo, Greifensee, Switzerland). Once the set-up was optimized, dissolution experiments were performed for neat HPMCAS and HPMCAS-based ASDs. Samples were taken using a 2 mL syringe needle which was inserted through a small hole in the polystyrene sheet. The media was replenished with fresh buffer maintained at 37 ºC and kept in another beaker under a polystyrene sheet. The pH was checked at the end of the experiment, and the data were considered for further evaluation only if pH showed a change of less than 0.1 units. Samples were analyzed using HPLC as described in sections 4.1 and 4.2.

4.6.Tiny-TIM

*4.6.1. Design and Set-up*

The tiny-TIM by The TIM Company (Delft, Netherlands) consists of a dynamic computer-controlled gastric compartment and small intestinal compartment to simulate the human gastro-intestinal system. The gastric and the intestinal compartments consist of a flexible silicon sleeve immersed in water maintained at 37°C, and contained within a glass jacket. Contraction and

distension are applied to the silicon sleeve via the external water compartment which has inlet and outlet valves, thereby mimicking gastrointestinal motility. A peristaltic valve controls the movement of mass and fluid from the gastric to small intestinal compartments. Air pressure applied on the valves permit opening or closing. There are two pH probes, one in stomach and one in the intestinal compartment to measure pH in real time. Throughout the experiment, pH curves are generated based on data gathered by the pH probes and are used to ensure physiological pH conditions are maintained via addition of acid or base when the pH deviates from pre-set values. The intestinal compartment is connected to a polysulfone hollow fiber membrane with a cut-off diameter of 50 nm which acts as a simulated absorption unit allowing the passage of dissolved species in the gastro-intestinal fluids. Samples passed through the polysulfone membrane are sampled continuously throughout the run based on weight, and samples are pooled together based on regular time intervals and are considered to be the bioaccessible fraction (fraction of the drug available for absorption). All media were prepared as per Table S2 and were filled into 8 syringes. The media were: fasted gastric enzyme solution, pancreatin solution, water, bile, 1 M HCl, sodium bicarbonate buffer, small intestinal electrolyte (SIES), and water to replenish the media in compartments when samples are taken. As per the predetermined protocol, different amounts of 1 M HCl and sodium bicarbonate are pumped into the system through syringes to adjust the pH throughout the experiments.

*4.6.2. Sampling and Run*

Before starting the experiment, 270 g of media was added into the gastric compartment. 1 mL of 2 mg/mL trypsin solution was added into the small intestine compartment. The hollow fiber membrane filter was rinsed with a solution containing ~9 mL bile, 16 mL 10% pancreatin and 65 mL SIES. Once the set-up was ready, the weighed amount of sample powder was added, and the

run commenced. The total run time for an experiment in the tiny-TIM was 5 hours. Samples were taken every 15 min for the 1st hour and every 30 minutes for the rest of the run. The housekeeping wave took place at the end of one hour, where all contents from the gastric compartment were mixed with into the intestinal compartment by opening of a peristaltic valve. Figure S2 shows the pH profiles measured by each pH probe in the stomach and small intestine during the course of entire tiny-TIM run. Samples in the collection vessel were analyzed with HPLC. Two runs were performed, one with 100 mg of crystalline ritonavir, and the second with a 100 mg drug dose using the RTV: HPMCAS 20% DL ASD (500 mg of total ASD). The particle size range of the crystalline drug and ASD powders was 106-250 μm (based on sieve fraction).

4.7. Determination of Equilibrium Surface pH: Slurry pH Method

The slurry pH method was adapted from Pudipeddi et al.[53] for determination of the equilibrium surface pH for HPMCAS-MF. Briefly, an excess amount (20-40% w/w above its solubility limit) of HPMCAS-MF was added to ultrapure water and vortexed for 15 minutes to create a slurry of HPMCAS-MF. The pH of the suspension was determined using a B10P benchtop pH meter (VWR International, Radnor, PA) with a connected sympHony combination pH probe (VWR International, Radnor, PA). The suspension showed a constant pH value within 15 minutes.

4.8. Determination of Boundary Layer pH gradient: Confocal Microscopy

Confocal fluorescence microcopy was used to image the boundary layer of a dissolving HPMCAS or ASD compact in situ and to quantify the boundary layer pH gradient as a function of distance from the solid-liquid interface.[54] Briefly, 0.1 % w/v of the fluorescein isothiocyanate (FITC), a pH-sensitive fluorescent dye, was dissolved in phosphate buffer of various pH ranging from 5.0 to 9.0. Images of each calibration sample of known pH containing FITC were obtained using the confocal microscope. From these, a calibration curve was prepared. Briefly, Image-J

software was used to determine the mean green intensity of the solutions of different pH, where a region of interest (ROI) was selected for each image, and a histogram of intensities was created. The region of interest was a rectangle of 100 µm in width and 1000 µm in height. To evaluate the pH gradient from neat polymer or ASD, a 100 mg compact of neat HPMCAS or RTV: HPMCAS 20% DL ASD was prepared from powder by compaction using a Carver press maintained at 1500 psi for one minute. The compact was adhered to the surface of a 14 mm diameter well plate by applying a miniscule amount of organic solvent to one surface with a brush and pushing into contact with the glass, followed by solvent evaporation. A thin layer of vacuum grease was applied to the top surface. Next, 3 mL of buffer containing 0.1% w/v FITC was added. The diameter of the compact was 8 mm and hence the remaining 6 mm of space in the well plate, containing the buffer was imaged using the confocal microscope. A Nikon R1 fluorescence microscope (Melville, NY) with a 20x lens was used. Images were taken every minute for 60 minutes. 14 ROIs were selected for each timepoint image, representing various locations of different distance from the dissolving interface. The same ROIs were used across all images and the average pH was determined for each ROI based on the calibration curve. Two controls were employed to confirm that there were no confounding detector or laser fluctuations. An inert weight of the same diameter as the ASD compact (8 mm) was adhered to a 14 mm well plate and buffer containing FITC was added. No change in intensity was observed over a 1 h period, confirming the stability of the laser and the fluorescent dye. Likewise, no detector fluctuations were observed when using a pH-insensitive dye, rhodamine-6G (R6G).

4.9.Gel Layer pH determination

The pH of the gel layer for a neat HPMCAS compact was determined following immersion in 50 mM pH 6.5 phosphate buffer as described previously.[3] In brief, a dispersion of HPMCAS and

chlorophenol red was prepared. After exposure to the dissolution medium, the surface gel layer was physically removed using a spatula and transferred to a glass slide. A Varian Cary 300 Bio (Varian, Inc., Palo Alto, CA, USA) UV-visible spectrophotometer was used to obtain the spectrum of the gel. The gel pH was determined using a calibration curve over the pH range 4.8-6.8 (R2 of 0.99) constructed using chlorophenol red solutions of known pH.

## 5. Results

### 5.1. Surface Area Normalized Dissolution Rate Experiments

Figure 2 shows a summary of surface area normalized release rates for neat HPMCAS and a 20% drug loading (DL) ASD of RTV with HPMCAS, performed in pH 6.5 phosphate buffer with molarities of 20 or 50 mM. These correspond to buffer capacities of 8.7 mM/ΔpH and 23.8 mM/ΔpH respectively. For both buffer molarities, drug and polymer released at similar normalized release rates from the ASD. The normalized release rates were of the same order of magnitude as the neat polymer release rate, indicating that the release was controlled by the polymer; neat lipophilic amorphous drugs release much slower than neat polymer.[55–57] The release rate of polymer from the ASD was lower than that of the neat polymer for both buffer molarities, but this decrease was more notable 50 mM buffer compared to 20 mM buffer. This is in line with previous observations, and has been attributed to a change in the predominant release mechanism as buffer capacity is altered.[3]

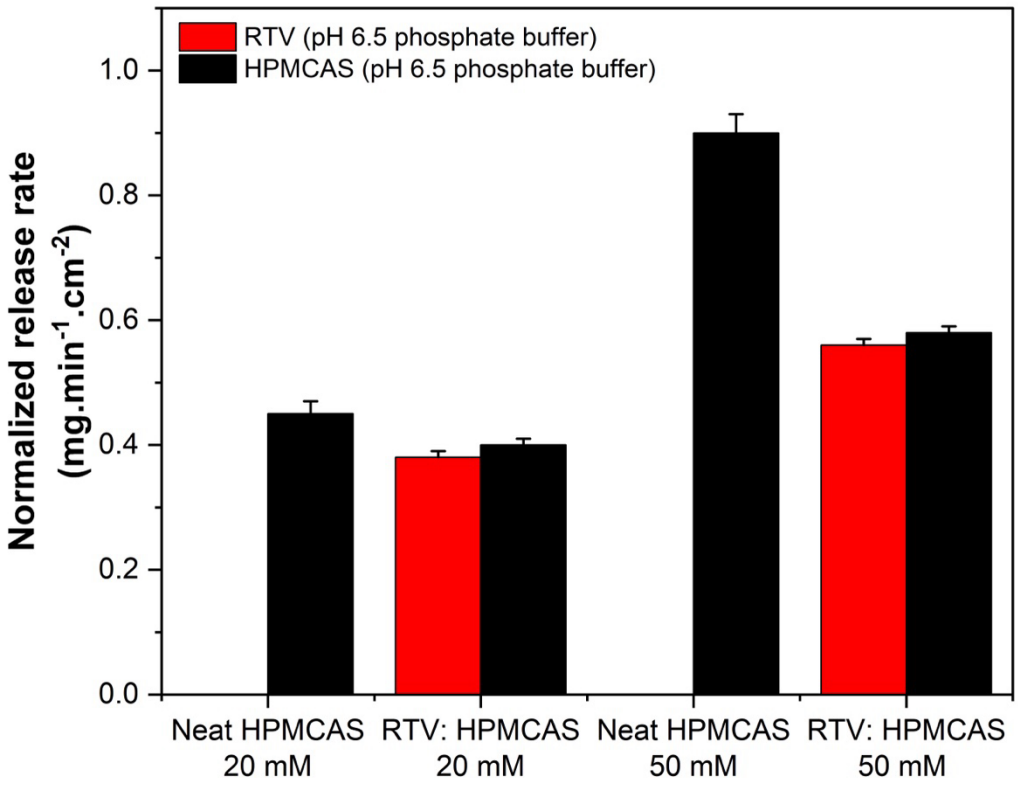


**Figure 2. Comparison of normalized release rates of neat HPMCAS and ASD components from RTV: HPMCAS 20:80 ASDs in pH 6.5 phosphate buffer 20 mM or 50 mM. Error bars represent standard deviations, n = 3.**

Surface normalized dissolution rates for neat polymer and components from the RTV: HPMCAS 20:80 ASD were also performed in 20 mM pH 6.5 bicarbonate buffer using the floating lid set up. Prior to conducting these experiments, pH stability was monitored to confirm that $CO_2$ loss was minimized using this approach. Figure 3 shows a comparison between the pH stability of the bicarbonate buffer system with and without the floating lid. It is apparent that good pH stability was achieved using the floating lid for the duration of the experiment, whereas the pH variation was unacceptable for the open system. 20 mM pH 6.5 bicarbonate buffer was chosen to provide a

comparable medium to that used in the tiny-TIM experiments, although the buffer concentration was much more dynamic in the latter system.

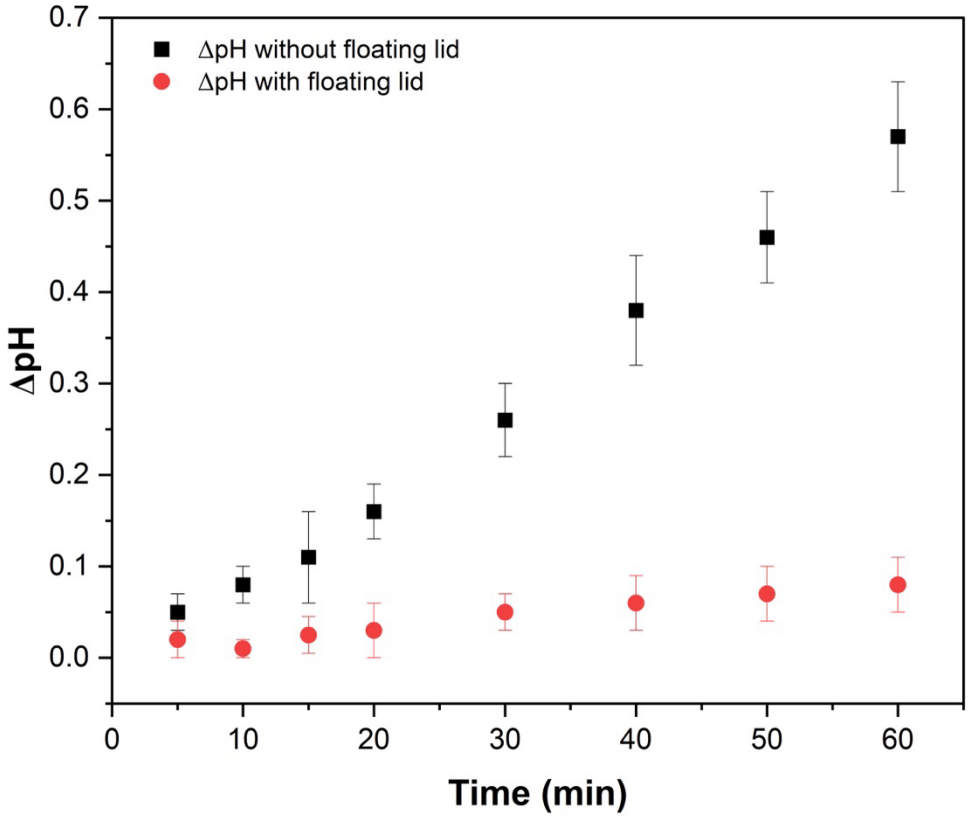


**Figure 3. Change in pH with and without floating lid in 20 mM pH 6.5 bicarbonate buffer. Error bars represent standard deviations, n = 3.**

Comparing bicarbonate and phosphate buffers of the same molar concentration and pH 6.5 (Figure 4) revealed slower release of neat HPMCAS and ASD components from the bicarbonate buffer. These data show that the release rate of RTV from the ASD in the 20 mM bicarbonate buffer was approximately 60% of that observed for the 20 mM phosphate buffer. Importantly, the polymer and drug released at the same normalized rate in bicarbonate buffer, indicating that the polymer dissolution controlled the drug release rate. Therefore, the mechanism of drug release

was unchanged when switching from phosphate to bicarbonate buffer, and was controlled by the polymer release in both media.

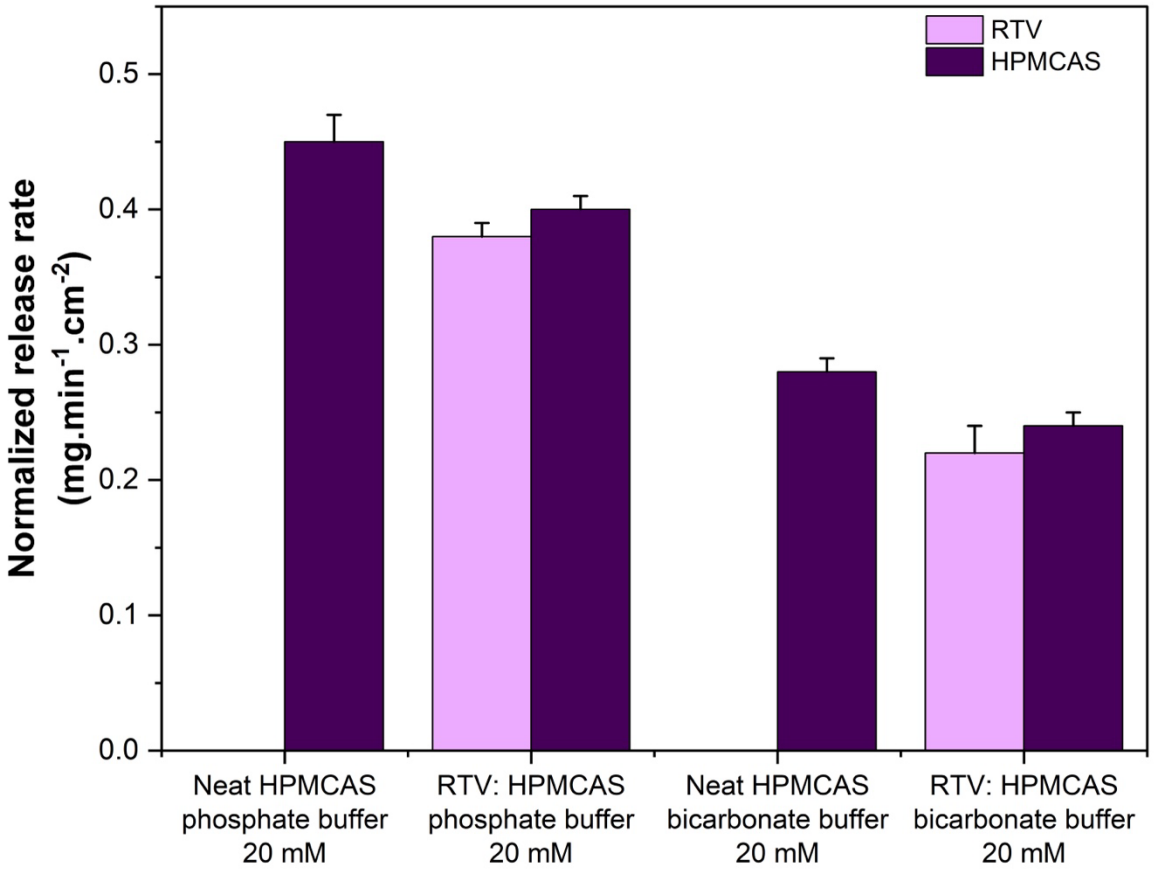


**Figure 4. Comparison of normalized release rates of neat HPMCAS and components from the RTV: HPMCAS 20:80 ASD in pH 6.5 20 mM phosphate and pH 6.5 20 mM bicarbonate buffer. Error bars represent standard deviations, n = 3.**

Figure 5 shows that the release rates of neat HPMCAS and the components of the RTV: HPMCAS ASD in 20 mM pH 6.5 bicarbonate buffer were very similar to the corresponding release rates in 10 mM pH 6.5 phosphate buffer. Further, Figure 6 shows that the release rates of neat HPMCAS and the components of the RTV: HPMCAS ASD in 10 mM pH 6.5 bicarbonate buffer were very similar to their release in 5 mM pH 6.5 phosphate buffer. At buffer molarities

of 5 mM, 10 mM and 20 mM, the normalized release rates of components from the ASDs were similar to the release rate of neat HPMCAS in the corresponding buffer for both phosphate and bicarbonate buffers.

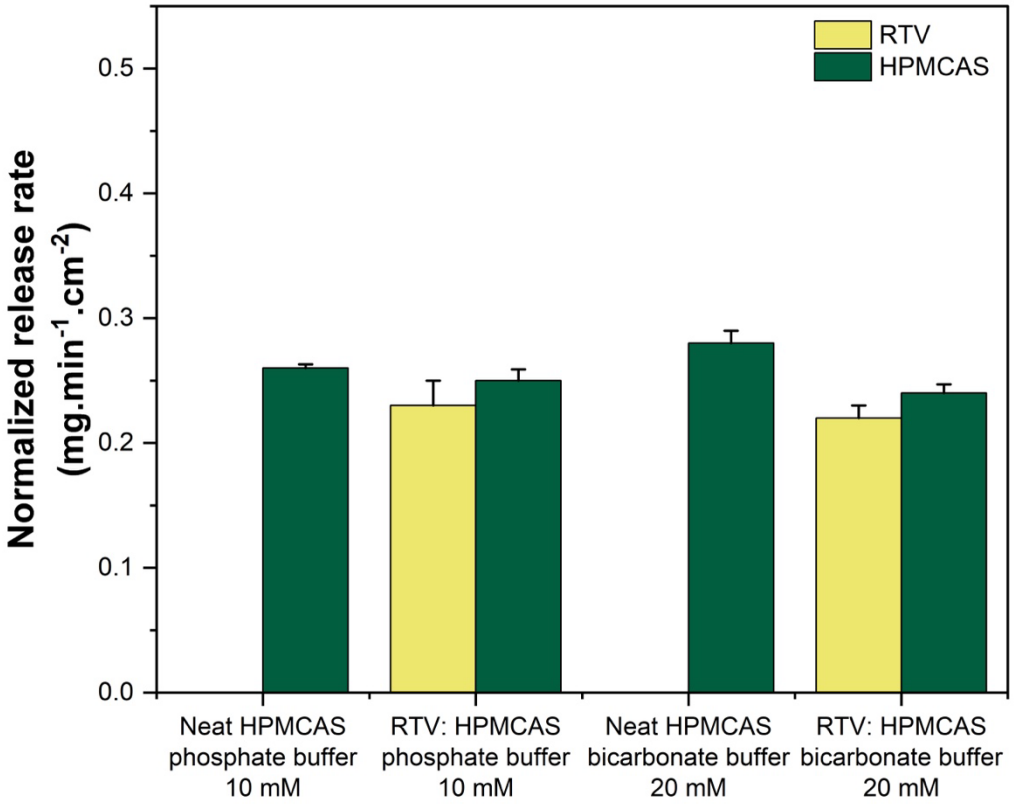


**Figure 5. Comparison of normalized release rates of neat HPMCAS and components from the RTV: HPMCAS 20:80 ASD in pH 6.5 10 mM phosphate (neat HPMCAS release rate value taken from Bapat et al.[3]) and pH 6.5 20 mM bicarbonate buffer. Error bars represent standard deviations, n = 3.**

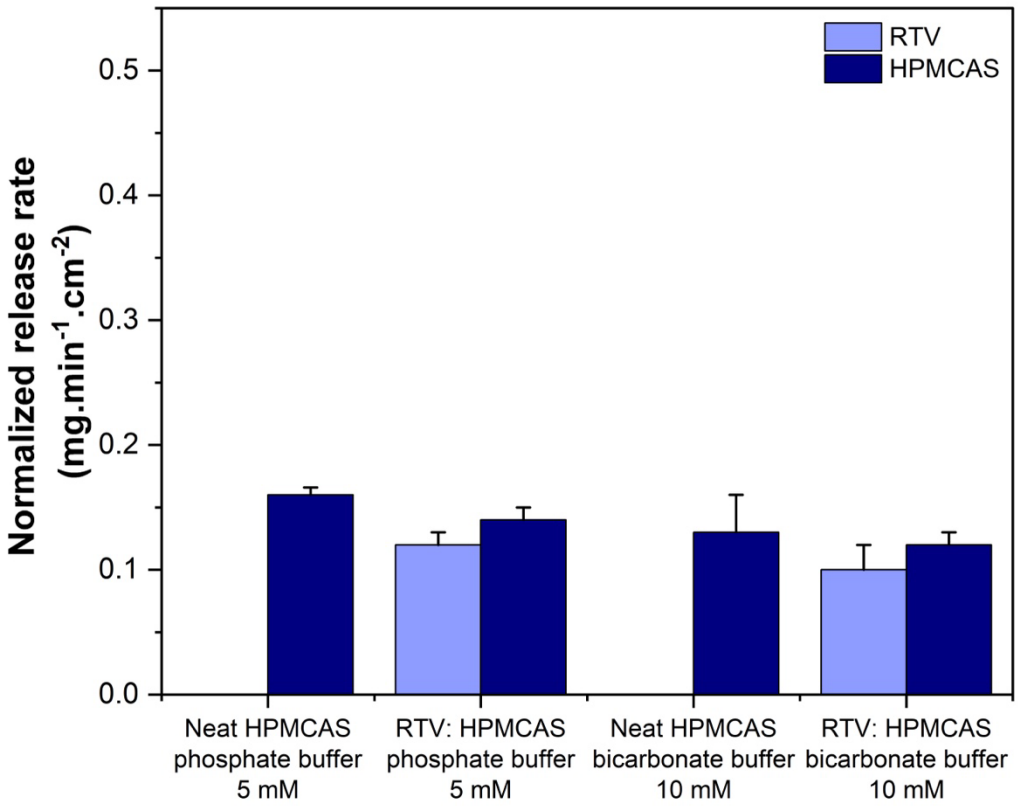


**Figure 6. Comparison of normalized release rates of neat HPMCAS and components from the RTV: HPMCAS 20:80 ASD in pH 6.5 5 mM phosphate (neat HPMCAS release rate value taken from Bapat et al.[3]) and pH 6.5 10 mM bicarbonate buffer. Error bars represent standard deviations, n = 3.**

5.2.Tiny-TIM results

Figure 7 shows the % of bioaccessible drug following dosing of 100 mg of crystalline RTV, or the RTV: HPMCAS 20:80 ASD to the tiny-TIM. The housekeeping wave occurred after one hour, whereby all contents were emptied into the intestinal compartment by opening of a peristaltic valve. Prior to the housekeeping wave, the amount of bioaccessible drug was low. Bioaccessibility of the ASD was about 5-fold higher as compared to the crystalline drug. For crystalline RTV, ~ 20% drug was bound to filter whereas for the ASDs ~40% filter binding was observed (Figure S3), in agreement with previous studies that show filter binding of RTV.[58] Thus, for the ASD, near mass balance is obtained where ~90% of the administered dose could either cross the membrane or bind to it, indicating a high degree of bioaccessibility and suggesting that most of the ASD could release. This is in accordance with the visual observation that all of the ASD powder had completely dissolved after 20 minutes when added to 20 mM pH 6.5 bicarbonate buffer during a powder dissolution experiment. In contrast, for the crystalline drug, <30% of the drug crossed or interacted with the membrane, suggesting that a large fraction remained undissolved at the end of the experiment. Table 2 shows a bioaccessibility estimation based on the crystalline and amorphous solubilities of RTV in FaSSIF. The estimated amount of bioaccessible drug based on solubility is >80% for the amorphous drug and <10% for the crystalline material, which is readily understandable based on the 8-fold difference in the solubilities of the two forms. The estimates in Table 2 are in agreement with experimental observations and support the conjecture that the bioaccessibility of crystalline RTV was solubility-limited whereas for the ASD, ~80% of the drug could dissolve based on the amorphous solubility and the available fluid volume.

**Table 2. Theoretical bioaccessibility estimation for a 100 mg dose based on crystalline and amorphous solubility values and available volume.**

| Sample | FaSSIF solubility* (mg/mL) | Fluid sampled in tTIM (mL) | Estimated mg bioaccessible | Actual mg bioaccessible |
|---|---|---|---|---|
| Crystalline RTV | 0.007* | 1412.8 | 9.9 | 8.9 |
| Amorphous RTV (RTV: HPMCAS ASD) | 0.058* | 1412.8 | 81.9 | 45.3 |

*Fluid in tiny-TIM intestinal compartment has a different composition from FaSSIF. Crystalline[59] and amorphous[60] solubility values were taken from the literature.

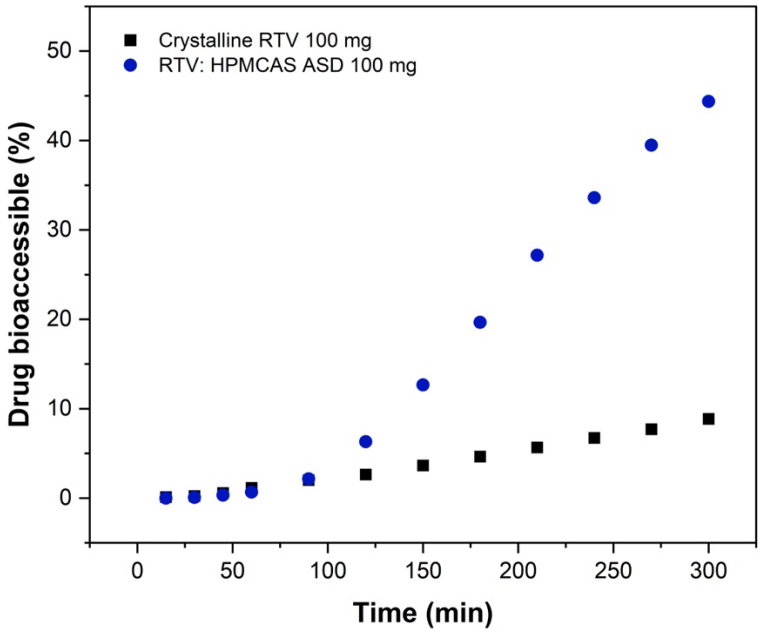


**Figure 7. Percent drug bioaccessible from tiny-TIM study for crystalline RTV, and RTV: HPMCAS 20:80 100 mg dose formulation.**

### 5.3. Boundary layer pH measurements for polymer and ASD compacts using confocal microscopy

FITC shows pH dependent fluorescence. 8A shows how the brightness of an aqueous solution of FITC, which emits green light, increases as the pH is increased. Figures 8B-C illustrate the procedure used to delineate a region of interest (ROI) and from this, measure the mean green intensity of the solutions of various pH values. From this procedure, a calibration curve over the pH range of 5.0-7.5 could be generated (Figure 8D). Figure 9 shows results from a control experiment where the pH was determined for a solution as a function of location and time, whereby an inert object (to mimic a tablet compact) was placed in the buffer. It is apparent that a consistent pH value was observed as a function of distance from the surface of the inert object (Figure 9A and Figure S4). Furthermore, the fluorescence intensity for a single ROI was constant over the duration of 1 h, indicating that the laser is sufficiently stable, and that FITC does not undergo photobleaching to an extent that could impact the results (Figure 9B and Figure S4). Similarly, the pH-insensitive dye, rhodamine 6G, showed no change in fluorescence intensity as a function of time and location (Figure S5 and Figure S6), again confirming sufficient stability of the laser and detector, to allow for dynamic experiments to be performed with confidence.

Following method optimization, similar experiments as a function of time and location were performed on neat HPMCAS compacts and RTV: HPMCAS ASDs compacts. The boundary layer pH gradient was then quantified for 14 constant ROIs, each of which had width of around 100 μm and a height of around 1000 μm, using pH 6.5 phosphate buffer of 20 mM or 50 mM. Figures 10 and 11 show representative fluorescence intensity images across the solution boundary layer for the two phosphate buffer solutions, and at different time points for neat HPMCAS. For both Figure 10 and 11, moving from left (adjacent compact surface) to right ("bulk solution"), it is apparent that the fluorescence intensity increased, indicating an increase in pH. Thus, even by qualitative examination, pH was clearly lower closer to the dissolving compact surface. With time, the low fluorescence intensity region extended further from the compact surface, which itself receded due to dissolution, although this was not seen directly from these images. At longer times, dissolution of the polymer resulted in a decrease in the "bulk" solution pH, due to the high amount of protons liberated during polymer dissolution and the limited volume of buffer relative to the mass of polymer. Therefore, quantitative evaluation of the pH gradient was performed only at a short times, where the extent of polymer dissolution was low. The pH gradients observed at 5 min are summarized in Figure 12A, while Figure 12B shows the development of the interfacial pH gradient as a function of time over the first 5 min. It is apparent that there was a steeper pH gradient between the surface and the bulk solution at the 5 min time point in 20 mM pH 6.5 phosphate buffer with a surface pH of 5.1 ± 0.1, whereas for 50 mM pH 6.5 phosphate buffer, the pH at the interface was 5.9± 0.1. The pH value approached that of the bulk solution at around 3 mm distance from the interface for the higher buffer capacity solution and at around 4 mm for the lower buffer capacity solution. The gel layer pH determined

using chlorophenol red in 50 mM pH 6.5 buffer was found to be 5.9± 0.1, in excellent agreement with the fluorescence method.

Figure 13 compares the pH profile of the boundary layer of a neat HPMCAS compact versus that of a RTV: HPMCAS 20:80 ASD compact as a function of distance from dissolving compact surface in 50 mM pH 6.5 phosphate buffer, after 5 min of exposure to buffer. It is clear that the presence of the drug did not impact the pH gradient.

A similar experiment on an RTV: HPMCAS ASD compact was performed in 20 mM pH 6.5 bicarbonate buffer for 5 minutes (Figure 12A). The mean green value for the ROI at the compact tablet-buffer interface showed a value of 0. This indicates that the interfacial pH was less than 5, since FITC shows no fluorescence below this value. The pH of a suspension of HPMCAS-MF in water, i.e. an unbuffered saturated solution was found to be 4.6 ± 0.1. Therefore, the pH at the interface for the bicarbonate buffer systems was between 4.6 and 5.0.

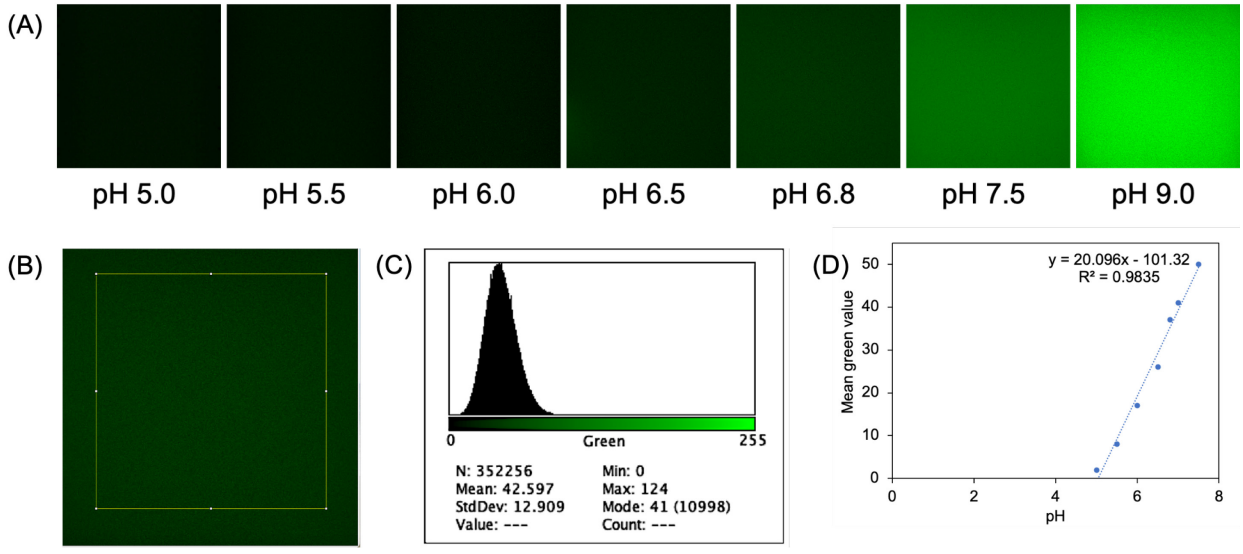


**Figure 8. Confocal images of FITC showing (A) fluorescence intensity in 50 mM phosphate buffer of various pH values, (B) an image with selected region of interest (ROI) on ImageJ software capturing a square with a side of 1000 μm, (C) mean green intensity calculated on ImageJ for selected ROI, and (D) calibration curve showing mean green intensity value as a function of pH for FITC for the calibration samples.**

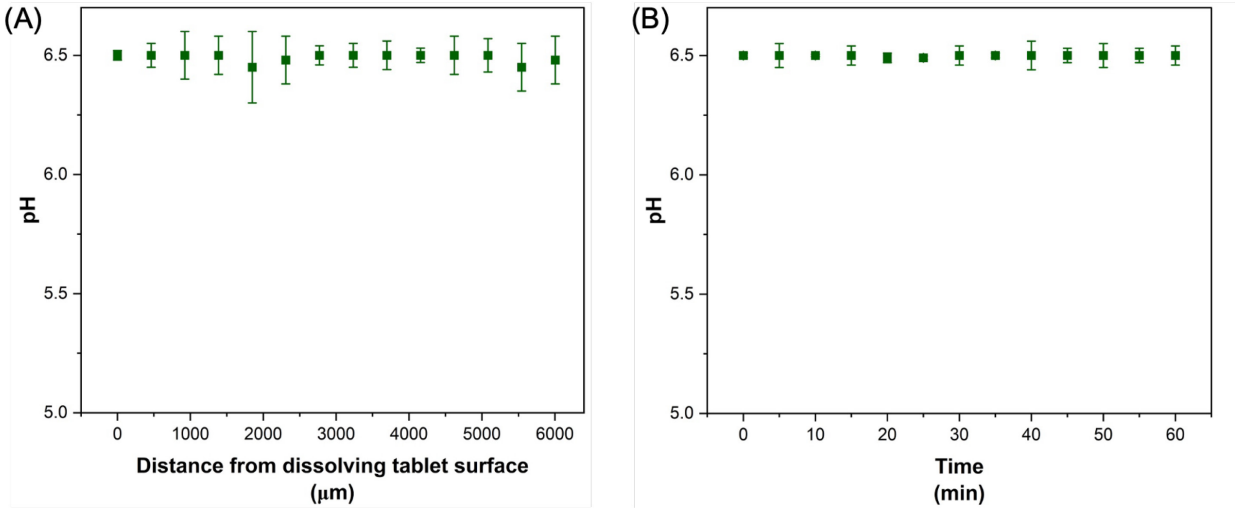


**Figure 9. Reference plot of pH stability from a confocal capture in 50 mM pH 6.5 phosphate buffer with added FITC around an inert object as a function of (A) distance from a dissolving compact surface and (B) time in minutes at a distance of around 3000 μm, confirming the absence of laser fluctuations. Error bars represent standard deviations, n = 3.**


**Figure 10. A confocal capture showing the entire boundary layer pH gradient at different time points (from top to bottom, 1, 2, 4 and 5 min) for a neat HPMCAS compact in 50 mM pH 6.5 phosphate buffer.**


**Figure 11. A confocal capture showing the entire boundary layer pH gradient at different time points (from top to bottom, 1, 2, 4 and 5 min) for neat HPMCAS compact in 20 mM pH 6.5 phosphate buffer.**

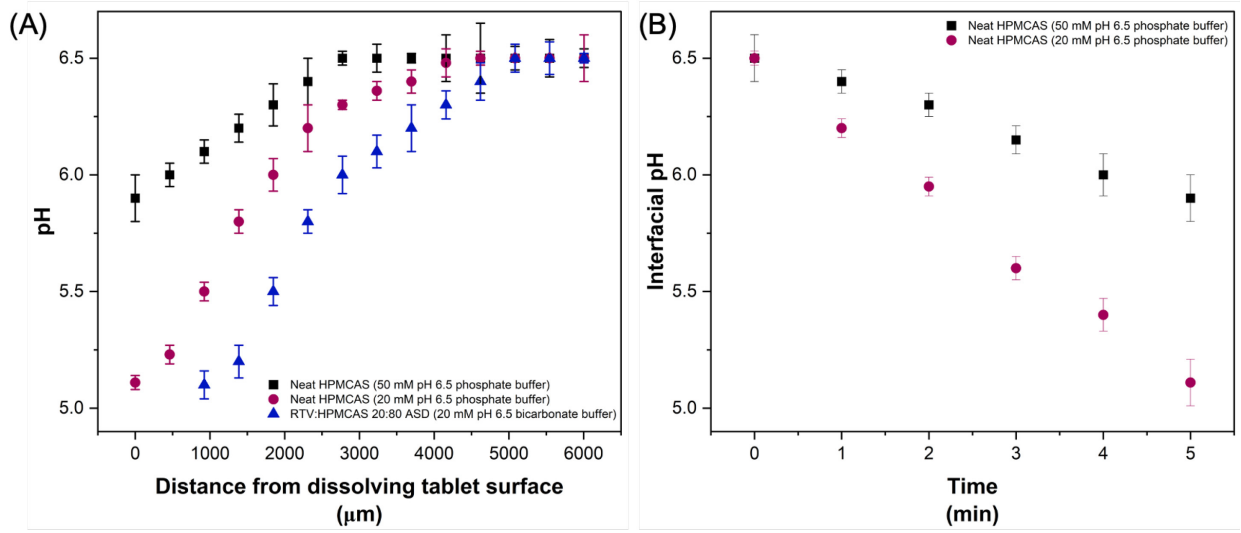


**Figure 12. (A) pH profile of boundary layer of a dissolving neat HPMCAS compact as a function of distance from dissolving compact surface in 50 mM and 20 mM pH 6.5 phosphate buffer with added FITC and the pH profile of boundary layer of a dissolving RTV: HPMCAS 20%DL ASD in 20 mM pH 6.5 bicarbonate buffer at 5 minutes, (B) interfacial pH of a dissolving neat HPMCAS compact as a function of time in 50 mM and 20 mM pH 6.5 phosphate buffer with added FITC. Error bars represent standard deviations, n = 3.**

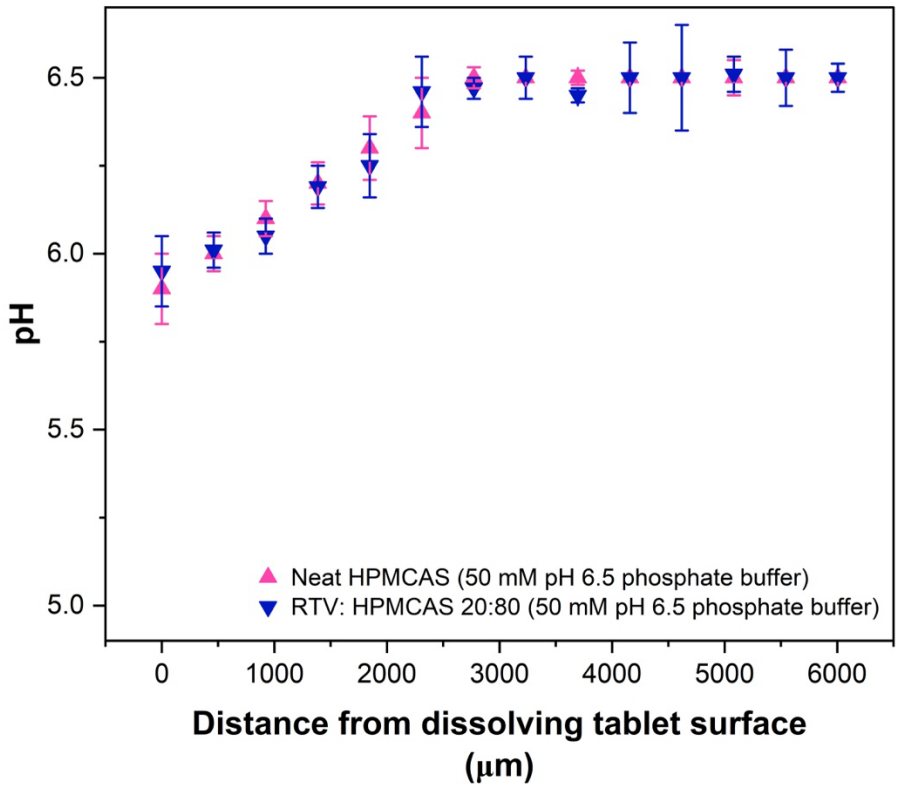


**Figure 13. pH profile of boundary layer of (A) a dissolving neat HPMCAS compact, (B) a dissolving RTV: HPMCAS 20:80 ASD compact as a function of distance from dissolving compact surface in 50 mM pH 6.5 phosphate buffer with added FITC. Error bars represent standard deviation, n = 3.**

## 6. Discussion

HPMCAS is one of the most widely used polymers in ASD formulations.[4,5,10,61] It is typically effective in inhibiting crystallization from the supersaturated solution generated upon ASD dissolution under non-sink conditions.[62–65] However, HPMCAS is an amphiphilic, ionizable polymer with pH-dependent solubility and therefore, has a pH-dependent dissolution rate.[3,14,17,18,55,62,66–68] Further, multiple studies have demonstrated that at drug loadings where the polymer is the majority component of the ASD, the polymer dissolution rate controls the release rate of the drug into solution.[8,20,69] Given the variability in pH and other media properties along

the gastrointestinal tract, understanding factors that impact the dissolution rate of HPMCAS, and consequently the drug release rate, are of thus of interest to enable optimized ASD formulations to be developed. In addition, understanding the relationship between HPMCAS/drug release rate, bulk solution pH and media composition is also critical to design meaningful in vitro testing approaches that predict release rates in vivo.

It is well known from classic studies of ionizable, crystalline small molecule APIs, that factors beyond the bulk solution pH control the dissolution rate.[70–72] The dissolution of a crystalline weakly acidic (or basic) compound is a diffusion-controlled process across an aqueous boundary layer, bounded on one side by the solid surface, and by the bulk solution on the other. The concentration gradients of drug and other species across the boundary layer result from diffusion of reactive species (from the surface to the bulk or from the bulk solution to the surface) and instantaneous reaction of acidic drug with water, hydroxyl ions and base components of the buffer. A critical parameter is the pH at the dissolving solid: solution interface, typically called the surface pH, which for an acid, is lower than the bulk solution pH. The surface pH of a crystalline drug depends on its intrinsic solubility, $pK_a$ and diffusion coefficient, as well as the concentration, diffusivity, pH and $pK_a$ of the buffer system.[71] For a weakly acidic compound, the reduction in surface pH relative to the bulk solution is due to dissociation and liberation of protons. The boundary conditions for the surface pH are the pH of a saturated solution of the drug in unbuffered media (lower bound),[70] and the bulk solution pH for scenarios where the acid is highly insoluble, or where the basic buffer species is present in such a high concentration that it swamps and controls the pH in the diffusion layer (upper bound).[71] There are multiple literature reports demonstrating that the surface pH of a weakly acidic compound is lower than the bulk solution pH, for pH ranges approximating small intestinal conditions and for acids with

$pK_a$ values of around 4-5.[70–73] In these instances, the surface pH was calculated from mathematical models, and validated by comparing the experimental and predicted dissolution flux.

Based on extensive studies on small molecules, the pH gradient observed for HPMCAS between the surface and the bulk aqueous solution (Figure 12) is to be expected, given the weakly acidic nature of the polymer, which has a reported $pK_a$ of 4.9,[20,22] and is in agreement with previous experimental and modeling studies on different acidic polymers.[28,74] The experimental surface pH observed in 50 mM phosphate buffer was 5.9± 0.1, while it was around 5.1± 0.1 in 20 mM phosphate buffer, for a bulk solution pH of 6.5 (Figure 12A). This difference in surface pH of 0.8 units accounts for the approximately two-fold difference in the intrinsic dissolution rate observed for neat HPMCAS in the two buffers (Figure 2). Although it would be of interest to compare the experimentally measured surface pH values to calculated values, unfortunately, the models used to calculate the surface pH of dissolving crystalline solids are likely not appropriate for predicting the surface pH of a dissolving polymer. This is because the interface between the solid surface and the boundary layer is not as well defined for a polymeric system, due to penetration of water and basic species into the polymer matrix, leading to polymer ionization and the formation of a thin gel layer at the surface. We have previously confirmed that HPMCAS does form a thin gel layer on the surface of a polymer compact in buffered aqueous media.[3] Consequently, there are at least two boundary layers which need to be considered: the gel layer (which is unlikely to be uniform in properties) and the aqueous boundary layer. Values for key parameters needed to calculate pH gradients, in particular diffusion coefficients of various species, cannot be estimated in the gel layer, since the viscosity is unknown, and likely to be non-uniform. Blechar et al. have pointed out other considerations specific to bicarbonate buffer

that also need to be considered in the case of gel layer formation and penetration of buffer species into the gel layer.[40]

From our current and past experimental studies,[3] we propose the schematic shown in Figure 14 to capture pH variations across the gel layer and aqueous boundary layer relative to the pH of the bulk solution.

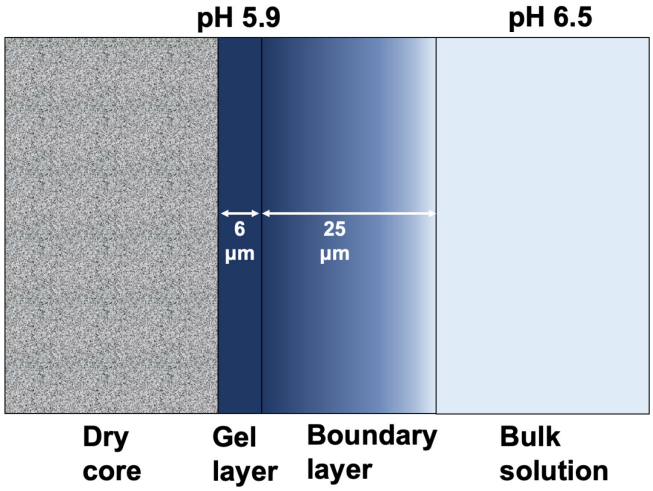


**Figure 14. Schematic showing the micro-environment of dissolving HPMCAS-MF/ASD compact in 50 mM pH 6.5 phosphate buffer.**

The interior of an HPMCAS compact is proposed to exist as a "dry" glass, consisting of unionized, or largely unionized HPMCAS that does not contain sufficient water to form a gel. HPMCAS has a dry glass transition temperature of 123°C, and has a large miscibility gap with water when unionized.[75] Gel formation requires sufficient water to be absorbed so that the polymer is extensively plasticized and mobilized. When enteric polymers become ionized, they are able to absorb larger amounts of water relative to the unionized polymer.[29] A gel layer thus forms between the glassy core and the aqueous boundary layer and consists of partially ionized polymer that is sufficiently hydrated and plasticized to form a gel layer, and which has sufficient viscosity to resist hydrodynamic forces. The apparent average pH of the gel layer of HPMCAS, which was reported to have a thickness of approximately 5-6 µm,[3] in pH 6.8 50 mM phosphate

buffer was 6.0.[3] For pH 6.5 50 mM phosphate buffer (conditions used in the current study), the gel layer pH was determined as pH 5.9± 0.1. The gel layer apparent pH, determined by incorporating a colorimetric pH indicator into the polymer, is in good agreement with the surface pH value of 5.9 ± 0.1 in 50 mM pH 6.5 phosphate buffer, estimated using an orthogonal method, namely a pH sensitive fluorescence probe (Figure 12). Because the surface pH value is lower than the bulk solution pH, a pH gradient exists across the aqueous boundary layer. The aqueous boundary layer thickness, calculated using the Levich equation,[76] is estimated as ~25 μm for a rotation speed of 100 rpm (conditions used for the rotating disc release studies shown in Figures 2, 4).

Comparing the surface pH in 20 mM phosphate versus 20 mM bicarbonate buffer (Figures 11, 12), it is apparent that a lower value is obtained in the latter buffer system. The actual value could not be determined but lies somewhere between 5.0 (lower limit of method) and 4.6 (pH of a saturated solution of HPMCAS, taken as the lower limit of the surface pH). This difference in surface pH explains why the intrinsic dissolution rate of both neat HPMCAS and release of components from the HPMCAS-RTV ASD are lower in 20 mM bicarbonate buffer than in 20 mM phosphate buffer (Figure 4). Sakamoto and Sugano found a similar magnitude of release difference for nifedipine from an HPMCAS-based ASD, when comparing bicarbonate and phosphate buffers of the same buffer capacity and pH.[39] It is likely that the surface pH differential between these two buffers is smaller than that between 20 and 50 mM phosphate buffer (ΔpH of 0.8), based on a consideration of the IDR ratios (factor of ~1.5 for 20 mM phosphate versus 20 mM bicarbonate, factor of ~2.2 for 50 mM versus 20 mM phosphate buffer). The relevant equations for dissolution flux which incorporate a consideration of surface pH differences can be found in Mooney et al.[71]

The lower surface pH observed for the HPMCAS-RTV ASD with 20 mM bicarbonate buffer relative to 20 mM phosphate buffer is consistent with observations from precedent-setting work with small crystalline organic acids. Krieg and coworkers demonstrated that the concentrations of phosphate buffer required to match the flux observed from physiologically relevant bicarbonate buffer (10.5 mM) were generally lowered.[73] For example, for ibuprofen, a phosphate buffer concentration of 4-8 mM was needed to match dissolution in the physiologically relevant bicarbonate buffer (10.5 mM), while for the less soluble acid, indomethacin, the corresponding phosphate concentration was estimated as 1-2 mM. Thus, based on the observations made in this study, as well the previous work of Krieg et al. comparing phosphate and physiologically relevant bicarbonate buffer, [73] it is clear that USP simulated intestinal buffer (50 mM phosphate buffer pH 6.8) would likely overpredict the dissolution rate of HPMCAS ASDs *in vivo*. Similarly, 20 mM phosphate buffer, which is closer to the buffer molarity used in FaSSIF (28 mM phosphate), led to a faster release rate than 20 mM bicarbonate buffer. However, 10 mM phosphate buffer matched the release rate of the ASDs in 20 mM bicarbonate buffer (higher end of physiologically relevant buffer molarity), while 5 mM phosphate buffer was a match for 10 mM bicarbonate buffer (which is around the bicarbonate buffer molarity typically considered as a good representation of physiological values[25,40,73]). Therefore, it may be reasonable to use these low molarity phosphate buffers to match physiologically relevant bicarbonate buffer for ASDs with HPMCAS MF grade. If the grade of HPMCAS used in the ASD is the less soluble HF grade, then a lower strength phosphate buffer is likely a more appropriate matching buffer, analogous to the situation described above with ibuprofen versus indomethacin. It is also important to note that the presence of the drug in the ASD was not found to impact the surface pH relative to the value observed for neat HPMCAS

(Figure 13). This is because the solubility of the drug is much lower than that of the polymer at the pH of interest.

Figure 4 demonstrates that the HPMCAS-RTV ASD has reasonable surface area normalized dissolution rates in physiologically relevant bicarbonate buffers. Because formulated commercial tablets containing HPMCAS ASDs tend to disintegrate when added to aqueous media, as long as the resultant ASD particle/agglomerate size is not too large, sufficient surface area should be available to enable complete release in a physiologically relevant time frame for this particular ASD system. Consequently, the RTV-ASD powder with a particle size range of 106-250 μm was observed to fully dissolve in 20 mM bicarbonate buffer in 20 min. This dissolution time is in accordance with the results of the tiny-TIM experiment which suggested that a majority of the RTV released from the ASD and was bioaccessible, in contrast to the crystalline powder. Thus, the tiny-TIM system predicts that RTV absorption is solubility limited in the case of crystalline drug, while ritonavir in the ASD, was rapidly released, even in biorelevant media, and hence, available for absorption. This is in broad agreement with an in vivo study comparing the absorption of crystalline ritonavir versus amorphous polyethylene glycol formulations in beagle dogs, where much higher area under the curve and maximum plasma concentration values were obtained for the amorphous formulations[10] when compared to crystalline ritonavir.

Al-Gousous et al. studied the rupture time of enteric coatings, comparing 8 mM bicarbonate buffer pH 6.5 to phosphate buffers of varying molarities and the same pH.[25] They found that 15 mM phosphate buffer most closely mimicked the rupture time observed in bicarbonate buffer. However, they studied different polymers, methacrylic acid-ethyl acrylate or polyvinyl acetate phthalate. As observed for different weakly acidic crystalline drugs, the molarity of phosphate buffer required to match a physiologically relevant bicarbonate buffer will be dependent on the

solubility of the polymer. Furthermore, these studies evaluate the rupture of a polymer coating, rather than polymer dissolution per se, whereby it is the polymer dissolution rate that is critically important for drug release from ASDs.

## 7. Conclusions

Release rates of drug and polymer from ritonavir-HPMCAS ASDs, as well as neat HPMCAS release rate were found to be highly dependent on buffer type and strength when assessed using a rotating disc apparatus. Release was slowest from physiologically relevant pH 6.5 10 mM bicarbonate buffer. Despite the slower release in bicarbonate buffer, ritonavir was found to be highly bioaccessible from the ASD powder when evaluated in the tiny-TIM apparatus. The slower release from bicarbonate buffer relative to phosphate buffer of the same molarity was attributed to a lower pH at the surface of the dissolving ASD in the former system. This was verified experimentally using confocal microscopy and a fluorescent probe that was sensitive to pH. These observations are in good agreement with studies of the variation in surface pH of weakly acidic crystalline drugs in different buffers.[73] The finding reported herein highlight important considerations for the in vitro assessment of HPMCAS-based ASDs. Thus, for drug loadings where polymer dissolution controls drug release, buffer type, pH and strength will influence release rates. Consequently, to predict in vivo outcomes, buffer properties should be matched to those of physiologically relevant bicarbonate buffer. For HPMCAS-MF grade ASDs, pH 6.5 phosphate buffer with molarity of 5-10 mM may meet this requirement. Clearly, these are preliminary observations, and additional ASD systems should be tested to compare release

properties in different buffers, and studies should be extended to include different HPMCAS grades and other enteric polymers of interest.

## 8. Acknowledgements

Boehringer Ingelheim Pharmaceuticals Inc. is thanked for providing funding for this study. The National Science Foundation is acknowledged for funding (DMR- 2204995).

## ASSOCIATED CONTENT

### Supporting Information

PXRD image of the ASD after preparation indicating its amorphous nature, pH profiles in stomach and small intestine during tiny-TIM runs, filter binding of RTV from crystalline RTV and RTV:HPMCAS ASD, ELSD gradient method details for analysis of HPMCAS, tiny-TIM media preparation details, confocal captures showing the entire boundary layer at different time points for an inert object in pH 6.5 phosphate buffer with dissolved fluorescein isothiocyanate (FITC) and dissolved rhodamine 6G (R6G) as references, reference plot of intensity stability from a confocal capture in pH 6.5 phosphate buffer with added rhodamine-6G around an inert object as a function of distance from a dissolving compact surface and time in minutes confirming absence of laser and detector fluctuation.

## 9. References


1. Beig A, Fine-Shamir N, Lindley D, Miller JM, Dahan A. Advantageous Solubility-Permeability Interplay When Using Amorphous Solid Dispersion (ASD) Formulation for the BCS Class IV P-gp Substrate Rifaximin: Simultaneous Increase of Both the Solubility and the Permeability. *AAPS J*. 2017;19(3):806-813. doi:10.1208/s12248-017-0052-1

2. Alonzo DE, Zhang GGZ, Zhou D, Gao Y, Taylor LS. Understanding the Behavior of Amorphous Pharmaceutical Systems during Dissolution. *Pharm Res*. 2010;27(4):608-618. doi:10.1007/s11095-009-0021-1

3. Bapat P, Paul S, Thakral NK, Tseng YC, Taylor LS. Does Media Choice Matter When Evaluating the Performance of Hydroxypropyl Methylcellulose Acetate Succinate-Based Amorphous Solid Dispersions? *Mol Pharmaceutics*. Published online September 26, 2023. doi:10.1021/acs.molpharmaceut.3c00586

4. Bhujbal SV, Mitra B, Jain U, et al. Pharmaceutical amorphous solid dispersion: A review of manufacturing strategies. *Acta Pharmaceutica Sinica B*. 2021;11(8):2505-2536. doi:10.1016/j.apsb.2021.05.014

5. Newman A, Knipp G, Zografi G. Assessing the performance of amorphous solid dispersions. *Journal of Pharmaceutical Sciences*. 2012;101(4):1355-1377. doi:10.1002/jps.23031

6. Newman A. Chapter 18 - Rational Design for Amorphous Solid Dispersions. In: Qiu Y, Chen Y, Zhang GGZ, Yu L, Mantri RV, eds. *Developing Solid Oral Dosage Forms (Second Edition)*. Academic Press; 2017:497-518. doi:10.1016/B978-0-12-802447-8.00018-2

7. Harmon P, Li L, Marsac PJ, McKelvey C, Variankaval N, Xu W. Amorphous solid dispersion: analytical chanllenges and opportunities. *AAPS Newsmagazine*. 2009;12:14-20.

8. Chen Y, Wang S, Wang S, et al. Initial Drug Dissolution from Amorphous Solid Dispersions Controlled by Polymer Dissolution and Drug-Polymer Interaction. *Pharm Res*. 2016;33(10):2445-2458. doi:10.1007/s11095-016-1969-2

9. Murdande SB, Pikal MJ, Shanker RM, Bogner RH. Solubility advantage of amorphous pharmaceuticals: I. A thermodynamic analysis. *Journal of Pharmaceutical Sciences*. 2010;99(3):1254-1264. doi:10.1002/jps.21903

10. Law D, Schmitt EA, Marsh KC, et al. Ritonavir–PEG 8000Amorphous Solid Dispersions: In vitro and In vivo Evaluations. *Journal of Pharmaceutical Sciences*. 2004;93(3):563-570. doi:10.1002/jps.10566

11. Law D, Krill SL, Schmitt EA, et al. Physicochemical considerations in the preparation of amorphous ritonavir–poly(ethylene glycol) 8000 solid dispersions. *Journal of Pharmaceutical Sciences*. 2001;90(8):1015-1025. doi:10.1002/jps.1054

12. Indulkar AS, Waters JE, Mo H, et al. Origin of Nanodroplet Formation Upon Dissolution of an Amorphous Solid Dispersion: A Mechanistic Isotope Scrambling Study. *Journal of Pharmaceutical Sciences*. 2017;106(8):1998-2008. doi:10.1016/j.xphs.2017.04.015

13. Jermain SV, Brough C, Williams RO. Amorphous solid dispersions and nanocrystal technologies for poorly water-soluble drug delivery – An update. *International Journal of Pharmaceutics*. 2018;535(1):379-392. doi:10.1016/j.ijpharm.2017.10.051

14. Vodak DT, Morgen M. Design and Development of HPMCAS-Based Spray-Dried Dispersions. In: Shah N, Sandhu H, Choi DS, Chokshi H, Malick AW, eds. *Amorphous Solid Dispersions: Theory and Practice*. Advances in Delivery Science and Technology. Springer; 2014:303-322. doi:10.1007/978-1-4939-1598-9_9

15. Almeida e Sousa L, Reutzel-Edens SM, Stephenson GA, Taylor LS. Assessment of the Amorphous "Solubility" of a Group of Diverse Drugs Using New Experimental and Theoretical Approaches. *Mol Pharmaceutics*. 2015;12(2):484-495. doi:10.1021/mp500571m

16. Bhugra C, Pikal MJ. Role of Thermodynamic, Molecular, and Kinetic Factors in Crystallization from the Amorphous State. *Journal of Pharmaceutical Sciences*. 2008;97(4):1329-1349. doi:10.1002/jps.21138

17. Curatolo W, Nightingale JA, Herbig SM. Utility of Hydroxypropylmethylcellulose Acetate Succinate (HPMCAS) for Initiation and Maintenance of Drug Supersaturation in the GI Milieu. *Pharm Res*. 2009;26(6):1419-1431. doi:10.1007/s11095-009-9852-z

18. Stewart AM, Grass ME, Brodeur TJ, et al. Impact of Drug-Rich Colloids of Itraconazole and HPMCAS on Membrane Flux in Vitro and Oral Bioavailability in Rats. *Mol Pharmaceutics*. 2017;14(7):2437-2449. doi:10.1021/acs.molpharmaceut.7b00338

19. Saboo S, Bapat P, Moseson DE, Kestur US, Taylor LS. Exploring the Role of Surfactants in Enhancing Drug Release from Amorphous Solid Dispersions at Higher Drug Loadings. *Pharmaceutics*. 2021;13(5):735. doi:10.3390/pharmaceutics13050735

20. Hiew TN, Zemlyanov DY, Taylor LS. Balancing Solid-State Stability and Dissolution Performance of Lumefantrine Amorphous Solid Dispersions: The Role of Polymer Choice and Drug–Polymer Interactions. *Mol Pharmaceutics*. 2022;19(2):392-413. doi:10.1021/acs.molpharmaceut.1c00481

21. Nguyen DA, Fogler HS. Facilitated diffusion in the dissolution of carboxylic polymers. Published online February 2005. doi:10.1002/aic.10329

22. Nguyen HT, Van Duong T, Taylor LS. Impact of Gastric pH Variations on the Release of Amorphous Solid Dispersion Formulations Containing a Weakly Basic Drug and Enteric Polymers. *Mol Pharmaceutics*. 2023;20(3):1681-1695. doi:10.1021/acs.molpharmaceut.2c00895

23. Amaral Silva D, Davies NM, Doschak MR, Al-Gousous J, Bou-Chacra N, Löbenberg R. Mechanistic understanding of underperforming enteric coated products: Opportunities to add clinical relevance to the dissolution test. *Journal of Controlled Release*. 2020;325:323-334. doi:10.1016/j.jconrel.2020.06.031

24. Dangel C, Kolter K, Reich Hb, Schepky G. Aqueous enteric coatings with methacryclic acid copolymer type C. Accessed February 22, 2022. https://www.elibrary.ru/item.asp?id=6096356

25. Al-Gousous J, Amidon GL, Langguth P. Toward Biopredictive Dissolution for Enteric Coated Dosage Forms. *Mol Pharmaceutics*. 2016;13(6):1927-1936. doi:10.1021/acs.molpharmaceut.6b00077

26. Spitael J, Kinget R. Solubility and dissolution rate of enteric polymers. *Acta Pharm Technol*. 1979;25(Suppl 7):163-168.

27. Karkossa F, Klein S. Assessing the influence of media composition and ionic strength on drug release from commercial immediate-release and enteric-coated aspirin tablets. *Journal of Pharmacy and Pharmacology*. 2017;69(10):1327-1340. doi:10.1111/jphp.12777

28. Ozturk SS, Palsson BO, Donohoe B, Dressman JB. Kinetics of Release from Enteric-Coated Tablets. *Pharm Res*. 1988;5(9):550-565. doi:10.1023/A:1015937912504

29. Qi Q, Taylor LS. Improved dissolution of an enteric polymer and its amorphous solid dispersions by polymer salt formation. *International Journal of Pharmaceutics*. 2022;622:121886. doi:10.1016/j.ijpharm.2022.121886

30. Klein S. The Use of Biorelevant Dissolution Media to Forecast the In Vivo Performance of a Drug. *AAPS J*. 2010;12(3):397-406. doi:10.1208/s12248-010-9203-3

31. Hens B, Tsume Y, Bermejo M, et al. Low Buffer Capacity and Alternating Motility along the Human Gastrointestinal Tract: Implications for in Vivo Dissolution and Absorption of Ionizable Drugs. *Mol Pharm*. 2017;14(12):4281-4294. doi:10.1021/acs.molpharmaceut.7b00426

32. Fadda HM, Sousa T, Carlsson AS, et al. Drug Solubility in Luminal Fluids from Different Regions of the Small and Large Intestine of Humans. *Mol Pharmaceutics*. 2010;7(5):1527-1532. doi:10.1021/mp100198q

33. Persson EM, Gustafsson AS, Carlsson AS, et al. The Effects of Food on the Dissolution of Poorly Soluble Drugs in Human and in Model Small Intestinal Fluids. *Pharm Res*. 2005;22(12):2141-2151. doi:10.1007/s11095-005-8192-x

34. Sheng JJ, McNamara DP, Amidon GL. Toward an In Vivo Dissolution Methodology: A Comparison of Phosphate and Bicarbonate Buffers. *Mol Pharmaceutics*. 2009;6(1):29-39. doi:10.1021/mp800148u

35. Garbacz G, Kołodziej B, Koziolek M, Weitschies W, Klein S. A dynamic system for the simulation of fasting luminal pH-gradients using hydrogen carbonate buffers for dissolution testing of ionisable compounds. *European Journal of Pharmaceutical Sciences*. 2014;51:224-231. doi:10.1016/j.ejps.2013.09.020

36. McNamara DP, Whitney KM, Goss SL. Use of a Physiologic Bicarbonate Buffer System for Dissolution Characterization of Ionizable Drugs. :6.

37. Al-Gousous J, Ruan H, Blechar JA, et al. Mechanistic analysis and experimental verification of bicarbonate-controlled enteric coat dissolution: Potential in vivo implications. *European Journal of Pharmaceutics and Biopharmaceutics*. 2019;139:47-58. doi:10.1016/j.ejpb.2019.03.012

38. Liu F, Merchant HA, Kulkarni RP, Alkademi M, Basit AW. Evolution of a physiological pH6.8 bicarbonate buffer system: Application to the dissolution testing of enteric coated products. *European Journal of Pharmaceutics and Biopharmaceutics*. 2011;78(1):151-157. doi:10.1016/j.ejpb.2011.01.001

39. Sakamoto A, Sugano K. Dissolution Kinetics of Nifedipine—Ionizable Polymer Amorphous Solid Dispersion: Comparison Between Bicarbonate and Phosphate Buffers. *Pharm Res*. 2021;38(12):2119-2127. doi:10.1007/s11095-021-03153-2

40. Blechar JA, Al-Gousous J, Wilhelmy C, Postina AM, Getto M, Langguth P. Toward Mechanistic Design of Surrogate Buffers for Dissolution Testing of pH-Dependent Drug Delivery Systems. *Pharmaceutics*. 2020;12(12):1197. doi:10.3390/pharmaceutics12121197

41. Sakamoto A, Izutsu K ichi, Yoshida H, Abe Y, Inoue D, Sugano K. Simple bicarbonate buffer system for dissolution testing: Floating lid method and its application to colonic drug delivery system. *Journal of Drug Delivery Science and Technology*. 2021;63:102447. doi:10.1016/j.jddst.2021.102447

42. Kalantzi L, Goumas K, Kalioras V, Abrahamsson B, Dressman JB, Reppas C. Characterization of the Human Upper Gastrointestinal Contents Under Conditions Simulating Bioavailability/Bioequivalence Studies. *Pharm Res*. 2006;23(1):165-176. doi:10.1007/s11095-005-8476-1

43. Sjövall H. Meaningful or redundant complexity – mechanisms behind cyclic changes in gastroduodenal pH in the fasting state. *Acta Physiologica*. 2011;201(1):127-131. doi:10.1111/j.1748-1716.2010.02155.x

44. Sarna SK, Otterson MF. Small Intestinal Physiology and Pathophysiology. *Gastroenterology Clinics of North America*. 1989;18(2):375-404. doi:10.1016/S0889-8553(21)00683-X

45. Clarysse S, Psachoulias D, Brouwers J, et al. Postprandial Changes in Solubilizing Capacity of Human Intestinal Fluids for BCS Class II Drugs. *Pharm Res*. 2009;26(6):1456-1466. doi:10.1007/s11095-009-9857-7

46. Verwei M, Minekus M, Zeijdner E, Schilderink R, Havenaar R. Evaluation of two dynamic in vitro models simulating fasted and fed state conditions in the upper gastrointestinal tract (TIM-1 and tiny-TIM) for investigating the bioaccessibility of pharmaceutical compounds from oral dosage forms. *International Journal of Pharmaceutics*. 2016;498(1):178-186. doi:10.1016/j.ijpharm.2015.11.048

47. Sarcevica I, Hens B, Tomaszewska I, McAllister M. Digitalizing the TIM-1 Model using Computational Approaches-Part One: TIM-1 Data Explorer. *Mol Pharm*. 2023;20(11):5416-5428. doi:10.1021/acs.molpharmaceut.3c00422

48. Preston SL, Piliero PJ, Bilello JA, Stein DS, Symonds WT, Drusano GL. In Vitro-In Vivo Model for Evaluating the Antiviral Activity of Amprenavir in Combination with Ritonavir Administered at 600 and 100 Milligrams, Respectively, Every 12 Hours. *Antimicrobial Agents and Chemotherapy*. 2003;47(11):3393-3399. doi:10.1128/aac.47.11.3393-3399.2003

49. Luo L, Thakral NK, Schwabe R, Li L, Chen S. Using Tiny-TIM Dissolution and In Silico Simulation to Accelerate Oral Product Development of a BCS Class II Compound. *AAPS PharmSciTech*. 2022;23(6):185. doi:10.1208/s12249-022-02343-4

50. Havenaar R, Anneveld B, Hanff LM, et al. In vitro gastrointestinal model (TIM) with predictive power, even for infants and children? *International Journal of Pharmaceutics*. 2013;457(1):327-332. doi:10.1016/j.ijpharm.2013.07.053

51. Hens B, Sarcevica I, Tomaszewska I, McAllister M. Digitalizing the TIM-1 Model Using Computational Approaches─Part Two: Digital TIM-1 Model in GastroPlus. *Mol Pharmaceutics*. 2023;20(11):5429-5439. doi:10.1021/acs.molpharmaceut.3c00423

52. López Mármol Á, Fischer PL, Wahl A, et al. Application of tiny-TIM as a mechanistic tool to investigate the in vitro performance of different itraconazole formulations under physiologically relevant conditions. *European Journal of Pharmaceutical Sciences*. 2022;173:106165. doi:10.1016/j.ejps.2022.106165

53. Pudipeddi M, Zannou EA, Vasanthavada M, et al. Measurement of Surface pH of Pharmaceutical Solids: A Critical Evaluation of Indicator Dye-Sorption Method and its Comparison With Slurry pH Method. *Journal of Pharmaceutical Sciences*. 2008;97(5):1831-1842. doi:10.1002/jps.21052

54. Cope SJ, Hibberd S, Whetstone J, MacRae RJ, Melia CD. Measurement and Mapping of pH in Hydrating Pharmaceutical Pellets Using Confocal Laser Scanning Microscopy. *Pharm Res*. 2002;19(10):1554-1563. doi:10.1023/A:1020425220441

55. Bapat P, Paul S, Tseng YC, Taylor LS. Interplay of Drug–Polymer Interactions and Release Performance for HPMCAS-Based Amorphous Solid Dispersions. *Mol Pharmaceutics*. 2024;21(3):1466-1478. doi:10.1021/acs.molpharmaceut.3c01106

56. Saboo S, Mugheirbi NA, Zemlyanov DY, Kestur US, Taylor LS. Congruent release of drug and polymer: A “sweet spot” in the dissolution of amorphous solid dispersions. *Journal of Controlled Release*. 2019;298:68-82. doi:10.1016/j.jconrel.2019.01.039

57. Saboo S, Moseson DE, Kestur US, Taylor LS. Patterns of drug release as a function of drug loading from amorphous solid dispersions: A comparison of five different polymers. *European Journal of Pharmaceutical Sciences*. 2020;155:105514. doi:10.1016/j.ejps.2020.105514

58. Hate SS, Reutzel-Edens SM, Taylor LS. Interplay of Adsorption, Supersaturation and the Presence of an Absorptive Sink on Drug Release from Mesoporous Silica-Based Formulations. *Pharm Res*. 2020;37(8):163. doi:10.1007/s11095-020-02879-9

59. Xu H, Krakow S, Shi Y, Rosenberg J, Gao P. In vitro characterization of ritonavir formulations and correlation to in vivo performance in dogs. *European Journal of Pharmaceutical Sciences*. 2018;115:286-295. doi:10.1016/j.ejps.2018.01.026

60. Niessen J, López Mármol Á, Ismail R, et al. Application of biorelevant in vitro assays for the assessment and optimization of ASD-based formulations for pediatric patients. *European Journal of Pharmaceutics and Biopharmaceutics*. 2023;185:13-27. doi:10.1016/j.ejpb.2023.02.008

61. McKelvey CA, Kesisoglou F. Enabling an HCV Treatment Revolution and the Frontiers of Solid Solution Formulation. *Journal of Pharmaceutical Sciences*. 2019;108(1):50-57. doi:10.1016/j.xphs.2018.11.003

62. Ueda K, Higashi K, Yamamoto K, Moribe K. The effect of HPMCAS functional groups on drug crystallization from the supersaturated state and dissolution improvement. *International Journal of Pharmaceutics*. 2014;464(1):205-213. doi:10.1016/j.ijpharm.2014.01.005

63. Ueda K, Higashi K, Kataoka M, Yamashita S, Yamamoto K, Moribe K. Inhibition mechanism of hydroxypropyl methylcellulose acetate succinate on drug crystallization in gastrointestinal fluid and drug permeability from a supersaturated solution. *European Journal of Pharmaceutical Sciences*. 2014;62:293-300. doi:10.1016/j.ejps.2014.06.007

64. Butreddy A. Hydroxypropyl methylcellulose acetate succinate as an exceptional polymer for amorphous solid dispersion formulations: A review from bench to clinic. *European Journal of Pharmaceutics and Biopharmaceutics*. 2022;177:289-307. doi:10.1016/j.ejpb.2022.07.010

65. Warren DB, Benameur H, Porter CJH, Pouton CW. Using polymeric precipitation inhibitors to improve the absorption of poorly water-soluble drugs: A mechanistic basis for utility. *Journal of Drug Targeting*. 2010;18(10):704-731. doi:10.3109/1061186X.2010.525652

66. Fukasawa M, Obara S. Molecular Weight Determination of Hypromellose Acetate Succinate (HPMCAS) Using Size Exclusion Chromatography with a Multi-Angle Laser Light Scattering Detector. *Chemical and Pharmaceutical Bulletin*. 2004;52(11):1391-1393. doi:10.1248/cpb.52.1391

67. Liu J, Li Y, Ao W, Xiao Y, Bai M, Li S. Preparation and Characterization of Aprepitant Solid Dispersion with HPMCAS-LF. *ACS Omega*. 2022;7(44):39907-39912. doi:10.1021/acsomega.2c04021

68. Tanno F, Nishiyama Y, Kokubo H, Obara S. Evaluation of Hypromellose Acetate Succinate (HPMCAS) as a Carrier in Solid Dispersions. *Drug Development and Industrial Pharmacy*. 2004;30(1):9-17. doi:10.1081/DDC-120027506

69. Simonelli AP, Mehta SC, Higuchi WI. Dissolution Rates of High Energy Polyvinylpyrrolidone (PVP)-Sulfathiazole Coprecipitates. *Journal of Pharmaceutical Sciences*. 1969;58(5):538-549. doi:10.1002/jps.2600580503

70. Mooney KG, Mintun MA, Himmelstein KJ, Stella VJ. Dissolution kinetics of carboxylic acids I: effect of pH under unbuffered conditions. *J Pharm Sci*. 1981;70(1):13-22. doi:10.1002/jps.2600700103

71. Mooney KG, Mintun MA, Himmelstein KJ, Stella VJ. Dissolution kinetics of carboxylic acids II: effect of buffers. *J Pharm Sci*. 1981;70(1):22-32. doi:10.1002/jps.2600700104

72. Palsson BO, Dressman JB, Ozturk. Dissolution of ionizable drugs in buffered and unbuffered solutions. *Pharm Res*. 1988;5(5):272-282. doi:10.1023/a:1015970502993

73. Krieg BJ, Taghavi SM, Amidon GL, Amidon GE. *In Vivo* Predictive Dissolution: Comparing the Effect of Bicarbonate and Phosphate Buffer on the Dissolution of Weak Acids and Weak Bases. *Journal of Pharmaceutical Sciences*. 2015;104(9):2894-2904. doi:10.1002/jps.24460

74. Harianawala AI, Bogner RH, Bradley M. Measurement of pH near dissolving enteric coatings. *International Journal of Pharmaceutics*. 2002;247(1):139-146. doi:10.1016/S0378-5173(02)00404-0

75. Dohrn S, Reimer P, Luebbert C, et al. Thermodynamic Modeling of Solvent-Impact on Phase Separation in Amorphous Solid Dispersions during Drying. *Mol Pharmaceutics*. 2020;17(7):2721-2733. doi:10.1021/acs.molpharmaceut.0c00418

76. Levich VG. Physicochemical hydrodynamics. Published online 1962.